Calculation of the transport properties of a dilute gas consisting of Lennard-Jones chains

Robert Hellmann, Nicolas Riesco, and Velisa Vesovic

Citation: J. Chem. Phys. **138**, 084309 (2013); doi: 10.1063/1.4793221
View online: http://dx.doi.org/10.1063/1.4793221
View Table of Contents: http://jcp.aip.org/resource/1/JCPSA6/v138/i8
Published by the American Institute of Physics.

Calculation of the transport properties of a dilute gas consisting of Lennard-Jones chains

Robert Hellmann,[1] Nicolas Riesco,[2,3] and Velisa Vesovic[3,a)]
[1]*Institut für Chemie, Universität Rostock, 18059 Rostock, Germany*
[2]*Qatar Carbonates and Carbon Storage Research Centre (QCCSRC), Imperial College London, London SW7 2AZ, United Kingdom*
[3]*Department of Earth Science and Engineering, Imperial College London, London SW7 2AZ, United Kingdom*

(Received 18 December 2012; accepted 7 February 2013; published online 28 February 2013)

The transport properties in the dilute gas limit have been calculated by the classical-trajectory method for a gas consisting of chain-like molecules. The molecules were modelled as rigid chains consisting of spherical segments that interact through a combination of site-site Lennard-Jones 12-6 potentials. Results are reported for shear viscosity, self-diffusion, and thermal conductivity for chains consisting of 1, 2, 3, 4, 5, 6, 7, 8, 10, 13, and 16 segments in the reduced temperature range of 0.3 − 50. The results indicate that the transport properties increase with temperature and decrease with chain length. At high temperatures the dependence of the transport properties is governed effectively by the repulsive part of the potential. No simple scaling with chain length has been observed. The higher order correction factors are larger than observed for real molecules so far, reaching asymptotic values of 1.019 − 1.033 and 1.060 − 1.072 for viscosity and thermal conductivity, respectively. The dominant contribution comes from the angular momentum coupling. The agreement with molecular dynamics calculations for viscosity is within the estimated accuracy of the two methods for shorter chains. However, for longer chains differences of up to 7% are observed. © *2013 American Institute of Physics*. [http://dx.doi.org/10.1063/1.4793221]

I. INTRODUCTION

The transport properties of a dilute gas can be related to the intermolecular forces between molecules by means of the kinetic theory.[1,2] The ability to relate the macroscopic properties of a gas to a molecular description has historically yielded a rich research seam. Numerous studies have been performed to elucidate what the dominant molecular interactions are that govern transport properties. However, the early studies were hampered by the lack of a full kinetic theory for polyatomic gases. Even when such a kinetic theory became available the complexity of the collisional dynamics made the calculation of transport properties computationally prohibitive.

One area that received sporadic attention was how the shape of a molecule influences transport properties. Initial work focused on models with a simple, but reasonably realistic intermolecular potential, that allow for the exact solution of the collisional dynamics. The resulting development of the kinetic theories of rough spheres[2,3] and loaded spheres[2,4–7] were the first attempts to study the effects of anisotropy and by proxy the effects of shape. This was followed by the pioneering work of Curtiss and co-workers[8–10] on the kinetic theory of spherocylinders. The collisions were approximated as collisions between two rigid bodies and the intermolecular potential was replaced by on-contact interactions. By introducing two dimensionless parameters, the eccentricity of the spherocylinder and a measure of the moment of inertia, they effectively accounted for the shape of a molecule and its mass distribution. Through a subsequent series of numerical simulations, Sandler and Dahler[11] were able to perform a systematic study of the dependence of transport properties of spherocylinders on these two parameters and hence provide a first indication of the role of the shape of molecules in determining transport properties.

The last few decades have seen major advances in our ability to calculate the transport properties of simple, dilute molecular gases directly from the full, *ab initio* intermolecular potential. Such calculations have been performed for a number of molecular systems: diatoms,[12,13] linear triatoms,[14–16] spherical tops,[17,18] and polar asymmetric tops.[19,20] The molecular collisions were computed by means of classical trajectories, while the full kinetic theory of polyatomic gases[1] has been used to calculate the transport properties. The accuracy of the calculated transport properties is generally commensurate with the best available experimental data. The usefulness of these calculations is specially evident at low and high temperatures, where experimental data are of lower accuracy or non-existent, and the current calculations can and do provide a better way of estimating transport properties. Although these studies have improved our insight into the dominant molecular processes that govern the transport properties, no systematic studies of the influence of the shape of molecules have been undertaken.

The recent advances have not been limited to dilute gases only. The developments in molecular dynamics (MD) have allowed for the calculations of transport properties to be performed over most of the phase space. However, the computational considerations and lack of accurate non-additive three-body potentials for most systems have limited a large number

a)Author to whom correspondence should be addressed. Electronic mail: v.vesovic@imperial.ac.uk.

of the molecular studies to the use of model intermolecular potentials. In principle, the accuracy of a molecular dynamics calculation can be tuned to a desired accuracy level. In practice, the computational resources limit the accuracy achievable, and in general for most molecular dynamics studies the accuracy is much lower than that routinely achievable by a combination of the kinetic theory and classical-trajectory calculations.

Galliéro and co-workers have carried out molecular dynamics simulations of ideal fluids to examine in a systematic manner their thermodynamic, interfacial, and transport properties,[21–24] and to quantify effects such as the hardness of the intermolecular potential,[25–29] molecular polarity,[30,31] shape,[32–34] and flexibility.[35] Ultimately, the use of these simplified models has allowed Galliéro and co-workers to formulate correlations for the estimation of the properties of real fluids.[22,30–32] Of particular significance to the present work are the studies reporting the viscosity[32] and thermal conductivity[33] of flexible Lennard-Jones (LJ) chains, which are currently being extended to rigid chains by Delage Santacreu *et al.*[35]

Recently, Patra and co-workers[36] have reported the viscosity and self-diffusion coefficients of two and three-dimensional Lennard-Jones chains of varying lengths and have examined how the dimensionality affects the transport properties of dense fluids. In a separate development, Yu and co-workers[37–39] have used Lennard-Jones chain fluids to generate equations to predict the self-diffusion of real fluids and in the process have relied on MD results in the dense fluid region. The work was recently extended to viscosity by means of the Stokes-Einstein relationship.[40] They have noted the lack of data for chains in the dilute gas limit, a gap that the current work is addressing.

Here, we take advantage of the recent developments in the classical-trajectory calculations to examine how the shape, or more precisely, the length of a molecule influences the transport properties of a dilute gas. We focus on a gas consisting of chain-like molecules that interact through a realistic soft, anisotropic intermolecular potential. In particular, we report on the shear viscosity, thermal conductivity, and the self-diffusion coefficient, the three transport properties that are weakly influenced by the anisotropy of the intermolecular potential.

II. THEORY

A. Intermolecular potential

The molecules are modelled as rigid chains consisting of n_s spherical segments, tangentially joined, each of mass m_s and diameter σ. Such chains, by definition, do not posses vibrational degrees of freedom and being linear have only two degrees of rotational freedom. We further assume that the chains interact through a combination of site-site intermolecular forces. The sites are placed at the center of each segment and therefore there would be n_s sites per chain. The choice of σ as the distance between neighboring sites is obviously not unique and was guided by the need to compare with molecular dynamics simulations. The site-site interaction is modelled by a simple LJ 12-6 potential. The potential is characterized by two parameters: the parameter σ defines the characteristic length at which the intermolecular potential is zero, while the parameter ϵ defines the characteristic energy that represents the well-depth of each site-site interaction potential. The choice of a Lennard-Jones 12-6 potential is not necessarily governed by how realistically it can represent the actual interaction between the real molecules, but by the fact that due to its simplicity it has been used by the molecular dynamics community to simulate transport properties of model systems, thus allowing us a comparison with the molecular dynamics results.

The effect of increasing the length of a rigid chain has two consequences. The anisotropy of the overall intermolecular potential, describing the interaction of two chains, will increase. The moment of inertia will also increase, leading to an easier exchange of the rotational and translational energy during collisions. Both the anisotropy and the inelastic collisions will have an effect on the transport properties of a gas.

B. Transport properties

The shear viscosity η, the product of the number density and the self-diffusion coefficient nD, and the thermal conductivity λ of a gas consisting of molecules represented by rigid chains can be expressed in the limit of zero density as

$$\eta = \frac{k_B T}{\langle v \rangle_0} \frac{f_\eta^{(n)}}{\mathfrak{S}(2000)}, \tag{1}$$

$$nD = \frac{k_B T}{m \langle v \rangle_0} \frac{f_D^{(n)}}{\mathfrak{S}'(1000)}, \tag{2}$$

$$\lambda = \frac{5 k_B^2 T}{2m \langle v \rangle_0} \frac{\mathfrak{S}(1001) - 2r\mathfrak{S}\binom{1001}{1010} + r^2 \mathfrak{S}(1010)}{\mathfrak{S}(1010)\mathfrak{S}(1001) - \mathfrak{S}\binom{1001}{1010}^2} f_\lambda^{(n)}, \tag{3}$$

where $\langle v \rangle_0 = 4(k_B T/\pi m)^{1/2}$ is the average relative thermal speed, k_B is Boltzmann's constant, m is the molecular mass, n is the number density, and T is the temperature. The parameter r is given by $r = (\frac{2}{5}\frac{c_{rot}}{k_B})^{1/2}$, where c_{rot} is the contribution of the rotational degrees of freedom to the isochoric heat capacity c_V. As the rigid chains are assumed to be linear, there are only two degrees of rotational freedom and as the calculation is done classically r^2 takes the value of 0.4. The quantities $\mathfrak{S}(2000)$, $\mathfrak{S}'(1000)$, $\mathfrak{S}(1010)$, $\mathfrak{S}(1001)$, and $\mathfrak{S}\binom{1001}{1010}$ are generalized cross sections. They include all of the information about the dynamics of the binary collisions that govern transport properties and in turn are governed by the intermolecular potential energy surface. The notation and conventions employed in labelling the generalized cross sections are fully described in Refs. 1, 14, and 17. The quantities $f^{(n)}$ are the nth-order correction factors that can be expressed in terms of generalized cross sections.[15,41–44] In this work, we have calculated up to the third-order correction factor for viscosity and up to the second order for thermal conductivity in line with our previous work.[17,18,45] No complete higher-order expressions for the self-diffusion coefficient have been developed

and hence we have calculated the product nD only in the first order, as given by Eq. (2) with $f_D^{(n)}$ set to unity. The higher-order correction factors, $f^{(n)}$, account for the effects of higher basis-function terms in the perturbation-series expansion of the solution of the Boltzmann equation.[1] As the expansion is performed both in the velocity and angular momentum space, one can distinguish two types of contributions to the higher-order correction factors. The velocity coupling in the second-order expansion for viscosity involves three basis functions (Φ^{2000}, Φ^{2010}, and Φ^{2001}), while that for thermal conductivity involves five basis functions (Φ^{10st}, $1 \leq s + t \leq 2$).[1,44] For the angular momentum expansion, a single additional basis function, Φ^{0200}, suffices for viscosity, while for thermal conductivity the expansion is performed by the inclusion of the tensorial basis function $\Phi^{1200|1}$. The complete expressions for higher order correction factors for viscosity and thermal conductivity are already available in the literature[15,17,43,44] and due to their length will not be given here.

If one considers the perturbation-series expansion in terms of total energy, rather than separating translational from internal energy as is done traditionally, one can derive a much simpler expression for thermal conductivity.[1,46–48] In this total-energy flux approach, originally proposed by Thijsse and co-workers,[46] the thermal conductivity in the first-order approximation is inversely proportional to a single cross section and is given by

$$\lambda^{10\mathrm{E}} = \frac{5k_\mathrm{B}^2 T}{2m\langle v\rangle_0}\frac{1+r^2}{\mathfrak{S}(10\mathrm{E})}, \tag{4}$$

where $\mathfrak{S}(10\mathrm{E})$ is a linear combination of the three cross sections used to describe the thermal conductivity in the two-flux approach,[1,46–48]

$$\mathfrak{S}(10\mathrm{E}) = \frac{1}{1+r^2}\left[\mathfrak{S}(1010) + 2r\mathfrak{S}\begin{pmatrix}1001\\1010\end{pmatrix} + r^2\mathfrak{S}(1001)\right]. \tag{5}$$

C. Reduced properties

The objective of this study is to examine the influence of the length of a molecule and the resulting intermolecular potential anisotropy on the transport properties. Therefore, in this work we refrain from calculating the absolute values of the transport properties of gases consisting of rigid chain-like molecules. This would have required fully defining the site-site potential by ascribing specific values to the parameters ϵ and σ together with a value for the mass of a segment, m_s. Instead we define reduced transport properties as follows:

$$\eta^* = \eta\frac{\sigma^2}{\sqrt{m_\mathrm{s}\epsilon}}, \quad (nD)^* = (nD)\sigma^2\sqrt{\frac{m_\mathrm{s}}{\epsilon}},$$

$$\lambda^* = \lambda\frac{\sigma^2}{k_\mathrm{B}}\sqrt{\frac{m_\mathrm{s}}{\epsilon}}. \tag{6}$$

The definition of the reduced transport properties is equivalent to that already used in the literature.[32,33] The reduced generalized cross sections $\mathfrak{S}^*\left(\begin{smallmatrix}p\,q\,s\,t\\p'q's't'\end{smallmatrix}\right)$ have been normalized with respect to $\pi\sigma^2$ and are functions of a reduced temperature T^* which is defined as $T^* = k_\mathrm{B}T/\epsilon$. It is important to note that this definition of reduced temperature, in terms of site-site well-depth, is only unique for a spherical potential. For non-spherical potentials, that arise for any chain-like molecule made up of more than one segment, both the well-depth and the parameter σ vary with orientation of the two chains. Hence, there are a variety of energy scaling parameters that one can employ. If the transport property is weakly dependent on anisotropy, it is more appropriate to use the well-depth of the spherically averaged component of the full intermolecular potential as the energy scaling parameter. However, this introduces its own complications and it could be justified only if the chain-like molecules were used to represent real molecules, such as alkanes.

D. Numerical evaluation of the generalized cross sections

The generalized cross sections for rigid Lennard-Jones chains were computed by means of classical trajectories using a modified version of the TRAJECT software code.[49] For a given total energy, translational plus rotational, classical trajectories describing the collision of two chains were obtained by integrating Hamilton's equations from pre- to post-collisional values (initial and final separation: 1000σ). The total-energy-dependent generalized cross sections can be represented as nine-dimensional integrals over the initial states. They were calculated for 29 values of the reduced total energy, $E^* = E/\epsilon$, ranging from 0.1 to 1000, by means of a simple Monte Carlo procedure, in which the initial states were generated utilizing pseudo-random numbers. At each energy up to 10^7 trajectories were computed. The number of trajectories had to be reduced significantly for low reduced energies, because the computational demand to achieve a sufficient accuracy for a given trajectory is increasing as the energy decreases. The final integration over the total energy to obtain the temperature-dependent generalized cross sections was performed using Chebyshev quadrature.

Taking into account the Monte Carlo errors of the generalized cross sections and the symmetry under time reversal of production cross sections, we estimate that the precision of the transport cross sections used in Eqs. (1)–(3) is of the order of 0.2%, while the precision of the production cross sections is of the order of 1%. At the level of transport properties this translates to a precision in the computed values of shear viscosity, self-diffusion, and thermal conductivity of the order of 0.2%, 0.2%, and 0.5%, respectively.

Tables of the shear viscosity, self-diffusion, and thermal conductivity coefficients calculated in this work as a function of temperature and chain length have been deposited with the Electronic Physics Auxiliary Publication Service.[50]

III. RESULTS

A. Viscosity

Figure 1(a) illustrates the behavior of the reduced viscosity as a function of the reduced temperature T^* for a number of selected chains of different length, while Figure 1(b) illustrates the behavior of the reduced viscosity as a function of the number of segments for a number of selected reduced

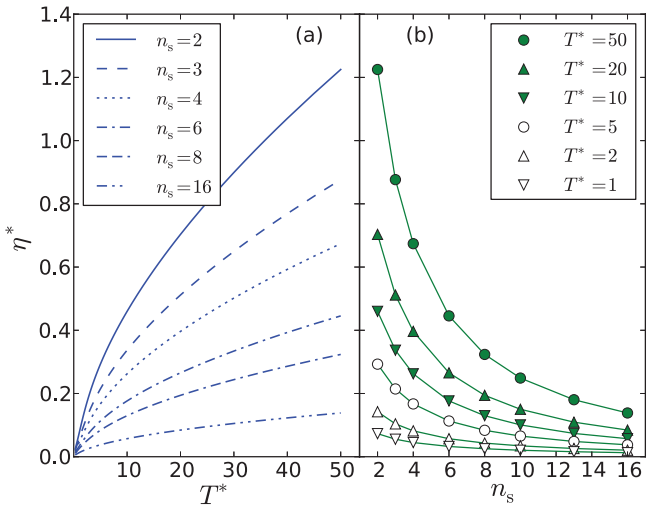

FIG. 1. Reduced viscosity η^* of rigid Lennard-Jones chains as a function of the reduced temperature T^* and the number of segments per chain n_s obtained using a third-order approximation.

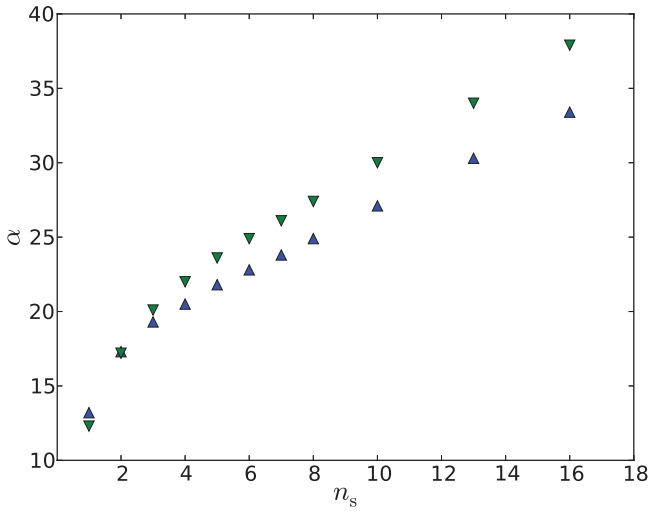

FIG. 2. Index α as a function of the number of segments per chain n_s obtained from fitting to the reduced viscosity η^* (▲) and to the product $(nD)^*$ (▼).

temperatures. The increase in the chain length leads to a decrease in the viscosity; the largest changes in the viscosity are observed for the shorter chains. At any particular reduced temperature, the decrease in viscosity does not obey any simple power law as a function of number of segments.

In their seminal work on evaluating transport property coefficients of fluids consisting of rigid spherocylinders, Sandler and Dahler[11] postulated that the observed decrease in the reduced viscosity, normalized with respect to the mass of a spherocylinder, can be solely attributed to the increase in the average projected area of a spherocylinder. Their finding was based on the analysis of the viscosity of spherocylinders of varying moments of inertia and eccentricity, but the longest spherocylinder examined corresponds to our 2-segment chain. For chains consisting of spherical segments the projected area, averaged over all orientations, A_{chain}, can be expressed as $A_{\text{chain}} = (\pi/4)\sigma^2 B(n_s) n_s$, where $B(n_s)$ is a slowly varying function of n_s. For a chain consisting of a single segment it takes a value of 1, for a 2-segment chain it is 0.925, for a 4-segment chain it is 0.887, while for an infinite chain length it asymptotically reaches a value of 0.849. Hence in a first approximation, we can assume that the function $B(n_s)$ is constant and the projected area, averaged over all orientations, is simply proportional to the number of segments, n_s. This is consistent with the argument of Sandler and Dahler[11] that the projected area of a spherocylinder, averaged over all orientations, is given by $(\pi/4)\sigma^2(1 + L/\sigma)$, where L is the length of a spherocylinder. If the decrease in viscosity is entirely due to a change in geometry, then the reduced viscosity η^*, normalized with respect to the mass of a segment, Eq. (6), should scale with $1/\sqrt{n_s}$. Our results indicate that this is in general not the case, although with a careful choice of a reference chain it can be made to work in a limited temperature range. For instance, the viscosity of the hexadecamer can be obtained within ±20% by scaling the viscosity of the tetramer, based on solely the increase of the projected area and of the mass. Hence, our results indicate that although the increases in average projected area and mass play an important part in reducing the viscosity, they are not, as Sandler and Dahler proposed, the sole effects. This may not be surprising since the generalized cross sections for hard-body potentials are proportional to the projected area, while those for more realistic soft potentials usually are not. The only way that the proportionality can be maintained is to allow the projected area to be temperature dependent, a development that was not explored in this work.

For all the chains studied the viscosity increases with temperature, while the rate of change decreases with increasing temperature as illustrated in Figure 1(a). At high reduced temperatures, corresponding to high collision energies, the repulsive wall of the intermolecular potential dominates the molecular interaction. For a purely repulsive, spherical intermolecular potential ($V \propto r^{-\alpha}$) it can be shown that the viscosity, in the first-order approximation, exhibits a $T^{(1/2+2/\alpha)}$ temperature dependence.[2] The analysis performed on the present results indicates that the viscosity, in the first-order approximation, of all the chains conforms to this temperature behavior in the range $5 < T^* < 50$. The goodness-of-fit, measured by the statistical parameter R, is better than 0.9994 for all the studied chains. Hence, at high temperatures, $T^* > 5$, the viscosity of the chain is determined by the effective repulsive potential. Figure 2 summarizes the hardness of the effective repulsive potential, measured by index α, for different chains.

As the chain length increases, so does the hardness of the effective repulsive wall. For a spherical LJ 12-6 potential the attractive part contributes up to very high energies. Hence, in the temperature range of interest here, the index α of the effective repulsive potential is not 12, but slightly higher. For viscosity, the dominant collisions occur at reduced energies of roughly $3T^*$.[51,52] The slope of the LJ 12-6 potential in the energy range $15 < V^* < 150$ is best described by the effective repulsive potential with an index α of about $13 - 14$. The analysis summarized in Figure 2 indicates that for a single sphere the viscosity is determined by the effective repulsive potential with an index α of 13.2. For longer chains, α

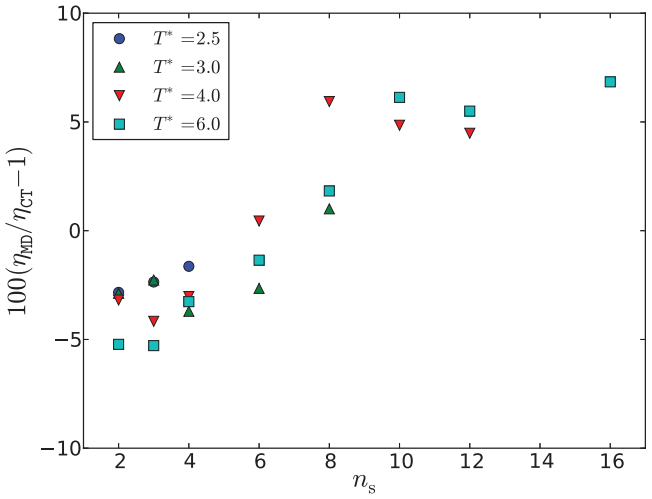

FIG. 3. Comparison of the reduced viscosity η^* of rigid Lennard-Jones chains obtained in this work (CT), calculated up to the third order, with those using molecular dynamics[35,58] (MD).

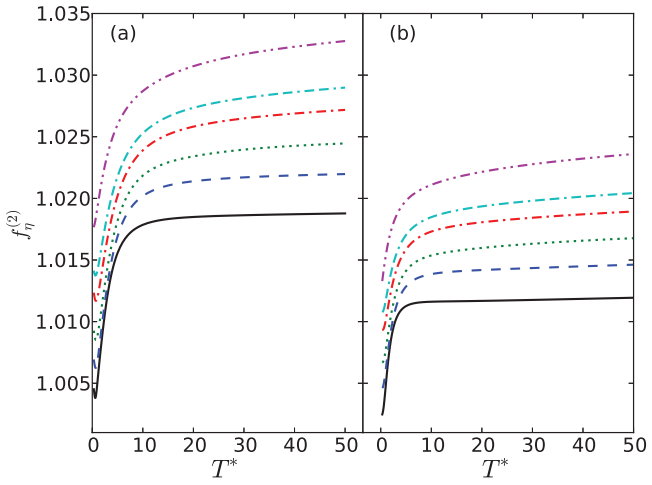

FIG. 4. (a) Second-order viscosity correction factor $f_\eta^{(2)}$ of rigid Lennard-Jones chains as a function of the reduced temperature T^*. (b) Contribution of the angular momentum coupling to the second-order viscosity correction factor: $n_s = 2$ (-), $n_s = 3$ (--), $n_s = 4$ (· ·), $n_s = 6$ (-· · -), $n_s = 8$ (--· ·), $n_s = 16$ (-· · ·).

increases to 23 for a chain consisting of 6 segments and to 33 for a chain consisting of 16 segments. For chains consisting of more than 3 segments, the index α of the effective repulsive potential increases essentially linearly with the number of segments. The importance of hard collisions, as the chain length and non-sphericity increase, has also been observed in recent studies of thermodynamic properties. The advances in the SAFT-Mie EOS[53–55] indicate that the larger molecules interact through a potential with increasingly more repulsive wall than the smaller and more spherical molecules. For instance, it has been reported that the power index of the repulsive part of the Mie potential used to represent alkanes increases from 15.6 for butane to 20.8 for dodecane.[56] Furthermore, recent studies,[57] based on the thermodynamic scaling of viscosity of alkanes, also support the observation that the steepness of the effective repulsive potential tends to increase with chain length.

As previously discussed, Delage Santacreu and coworkers[35] have also computed the zero-density viscosity of rigid chains interacting through site-site LJ 12-6 potentials, but using molecular dynamics. The simulations were performed at four reduced temperatures in the range $2.5 < T^* < 6$ for 2, 3, 4, 6, 8, 10, 12, and 16 segment chains. The values have been recently superseded by new, more accurate values of zero-density viscosity that are currently unpublished.[58] As we have not performed classical-trajectory calculations for 12 segments, we have interpolated our results as a function of chain length to estimate the reduced viscosity at the two highest temperatures. Figure 3 illustrates the deviation of the reduced viscosity obtained by the MD simulations[58] from those of the present paper. The agreement is good, all the deviations lie within the claimed accuracy of the MD results of 5%, except for longer chains where deviations of up to 7% are observed. However, for the higher reduced temperatures one can discern a systematic trend, even for shorter chains. For longer chains, the systematic trend persists leading to a viscosity of the hexadecamer obtained by MD simulations that is 6.8% higher than the current results. As the accuracy of the current CT calculation is more than an order of magnitude better than that of the MD calculation, it is likely that the systematic trend can be attributed to the combination of the MD calculations and approximations used to obtain an MD value at zero density.

We next consider the contribution of the higher-order correction factor $f_\eta^{(n)}$ to the shear viscosity. Figure 4(a) illustrates the temperature dependence of the second-order viscosity correction factors $f_\eta^{(2)}$ for a number of selected chains of different length. At low reduced temperatures $f_\eta^{(2)}$ increases rapidly, before beginning to level off in the region $5 < T^* < 10$. The magnitude of the correction increases with the chain length, which is a direct result of the increase in the non-sphericity of the potential. For the hexadecamer, the longest chain studied in this work, the second-order correction factor reaches a value of approximately 1.032 at the highest temperature. The major contribution to the second-order viscosity correction factor comes from the angular momentum coupling that also governs the viscosity decrease in the presence of an external magnetic field. Figure 4(b) illustrates that the second-order viscosity correction factor due to angular momentum coupling exhibits a similar behavior as the overall correction factor, increasing with increasing temperature and increasing chain length and reaching a value of 1.024 for the longest chain.

The overall behavior can be attributed to the non-sphericity of the potential and its differing influence on transport of linear and angular momentum. The anisotropy of the potential increases with increasing chain length, making it easier to induce changes in the angular momenta of the chains through collisions. This also leads to a stronger coupling between angular momentum and velocity. The result is that both cross sections $\mathfrak{S}(0200)$ and $\mathfrak{S}\binom{2000}{0200}$ increase rapidly with increasing chain length. According to the current calculations, the two cross sections increase roughly at the same rate. The second-order correction factor due to the angular momentum

coupling, given by

$$f_\eta^{(0200)} = \left[1 - \frac{\mathfrak{S}\binom{2000}{0200}^2}{\mathfrak{S}(2000)\mathfrak{S}(0200)}\right]^{-1}, \qquad (7)$$

is thus governed primarily by the ratio of the production cross section and the viscosity transport cross section, i.e., $\mathfrak{S}\binom{2000}{0200}/\mathfrak{S}(2000)$. The influence of the change in angular momentum is, as expected, much smaller for the viscosity cross section $\mathfrak{S}(2000)$ than for the production cross section. Thus, the increasing chain length, which leads to increasing non-sphericity, will result in an increase in the ratio $\mathfrak{S}\binom{2000}{0200}/\mathfrak{S}(2000)$ explaining qualitatively the observed behavior of the second-order viscosity correction factor as illustrated in Figure 4(b).

The second-order viscosity correction factor, illustrated in Figure 4(a), shows essentially the same qualitative behavior with temperature as observed for real polyatomic gases. However, its magnitude, especially at high reduced temperatures, is much larger than has been previously observed. The largest molecule studied so far, using an *ab initio* intermolecular potential, was CO_2.[14] For CO_2, the higher order viscosity correction factor reaches a maximum value of 1.011 at the highest temperature studied, while for N_2 and CO the maximum reached is of the order of 1.007.[12,13] It is difficult to make a direct comparison between the anisotropy of CO_2 and the site-site potential surfaces employed in this work. However, the ratio of the CO bond length (0.116 nm) to the value of σ (0.3 nm), based on the approximate size of the carbon and oxygen atoms is about 0.4. This is much smaller than the ratio of 1 used in this work for the chain-like molecules, indicating that using this simple measure of anisotropy the full *ab initio* CO_2 potential is less anisotropic than our 2-segment chain. Hence, it may be not surprising that the magnitude of the second-order viscosity correction factor for chain-like molecules is larger than was observed for real molecules so far.

For molecules interacting through a purely repulsive potential of the type described previously, it is also possible to calculate the second-order velocity correction factor for viscosity.[2] The magnitude of the correction factor is solely a function of the hardness of the potential, measured by the index α, and is independent of temperature. The near temperature independence of the second-order velocity correction factor calculated in this work further supports our earlier statement that at high temperatures the repulsive wall of the intermolecular potential dominates the collision dynamics. Furthermore, if one uses the effective values of the index α, reported in Figure 2, to calculate the second-order velocity correction factor for a repulsive potential, one obtains values of 1.0085, 1.0100, and 1.0115 for 2, 6, and 16 segment chains, respectively. This compares reasonably well with the values of 1.0068, 1.0083, and 1.0092 obtained in this work at $T^* = 50$.

The third-order viscosity correction factors are very similar to the second-order ones. Differences of at most 0.05% are observed, thus showing that even for a very highly non-spherical intermolecular potential the basis function expansion in velocity converges very rapidly.

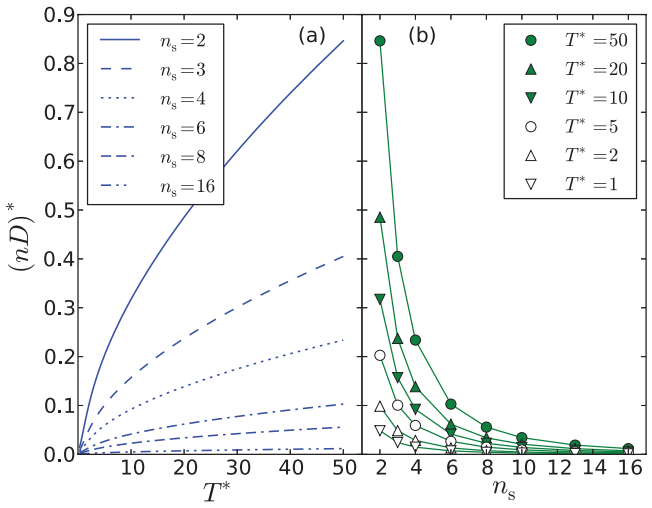

FIG. 5. Reduced self-diffusion coefficient of rigid Lennard-Jones chains as a function of the reduced temperature T^* and the number of segments per chain n_s.

B. Self-diffusion coefficient

Figure 5(a) illustrates the behavior of the reduced product of number density and the self-diffusion coefficient, $(nD)^*$, as a function of the reduced temperature T^* for a number of selected chains of different length, while Figure 5(b) illustrates the behavior of the product $(nD)^*$ as a function of the number of segments for a number of selected reduced temperatures. We observe similar behavior to that of viscosity. The increase in the chain length leads to a decrease in the product $(nD)^*$. Depending on temperature, the hexadecamer diffuses 100–220 times slower than a single monomer. No simple power law dependence on number of segments can account for this behavior, either overall or at a given reduced temperature.

Similar to the viscosity, the product $(nD)^*$ increases with temperature with the most rapid change observed for the shortest chain. The high reduced temperature behavior, $5 < T^* < 50$, can be accurately described by a $T^{(1/2+2/\alpha)}$ temperature dependence exhibited by repulsive intermolecular potentials. The goodness-of-fit as measured by the statistical parameter R is better than 0.9993 for all the chains studied. Hence, similar to viscosity, at high temperatures the self-diffusion of the chain is determined by the effective repulsive potential. Figure 2 summarizes the hardness of the effective repulsive potential, measured by the index α, for different chains. It can be observed that the effective repulsive potential describing $(nD)^*$ is marginally softer than the analogous effective viscosity potential. This is not too unexpected as the dominant collisions that contribute to the self-diffusion coefficient come from lower energies[51,52] than those for viscosity and consequently probe regions of the potential where the effect of the attractive contribution slightly softens the potential. However, the difference between the two effective potentials at the level of transport properties is marginal. Making

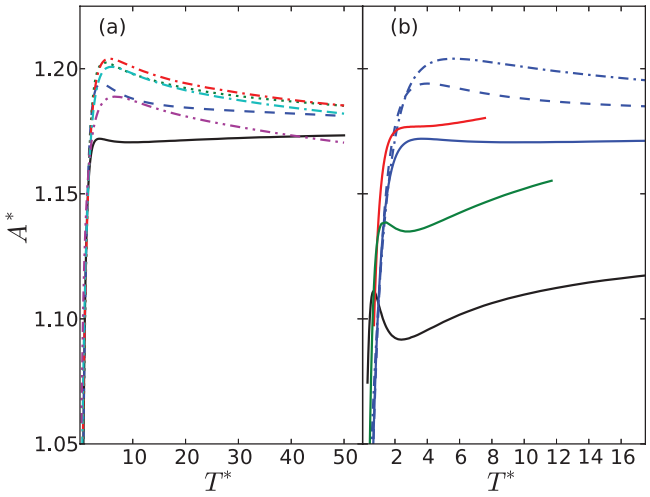

FIG. 6. (a) Parameter A^* of rigid Lennard-Jones chains as a function of the reduced temperature T^*: $n_s = 2$ (-), $n_s = 3$ (--), $n_s = 4$ (· ·), $n_s = 6$ (- · -), $n_s = 8$ (-- ·), $n_s = 16$ (- · ·). (b) Comparison of the parameter A^* for Lennard-Jones spheres (black solid line), CO_2 (red solid line), and CH_4 (green solid line) with that for Lennard-Jones chains (blue lines): $n_s = 2$ (-), $n_s = 3$ (--), $n_s = 6$ (- · -).

use of the index α obtained from $(nD)^*$ to calculate the temperature dependence of the reduced viscosity would result in an additional $1\% - 2\%$ error in viscosity.

C. Parameter A^*

Numerous studies indicate that diffusion coefficients and viscosity have a similar temperature dependence[59] and hence it is of interest to examine their ratio. It is customary in kinetic theory to do this by defining the dimensionless parameter A^* as[59]

$$A^* = \frac{5}{6}\frac{\mathfrak{S}(2000)}{\mathfrak{S}'(1000)}. \tag{8}$$

Figure 6 illustrates the behavior of the ratio A^* as a function of the reduced temperature T^* for a number of selected chains of different length. At low temperatures, the ratio A^* increases rapidly with temperature before levelling off at reduced temperatures of approximately $T^* = 1.0 - 3.0$, the exact value increasing with increasing chain length. As has already been observed, even for weakly non-spherical molecules,[14,17,45] the ratio A^* at higher reduced temperatures is a few percent higher than that obtained for molecules interacting through a spherical intermolecular potential. The increasing non-sphericity of the potential (i.e., increasing chain length) has a marginal influence on the magnitude of A^*. In fact for any chain consisting of more than 3 segments the variation of A^* is less than 1% for reduced temperatures T^* above 1. The weak dependence of A^* on the non-sphericity of the potential indicates that the non-spherical nature of the potential impacts in a similar way both the viscosity cross section $\mathfrak{S}(2000)$ and the self-diffusion cross section $\mathfrak{S}'(1000)$. The observed increase in the magnitude of A^* for chains compared to spheres can thus be attributed to the importance of the inelastic, rotational-translational energy exchanges. Most of the evidence comes from calculations using the Mason-Monchick approximation (MMA)[17,60–62] that use a full anisotropic potential, but ignore the impact of rotational-translational energy exchange. The MMA calculated viscosity is always closer to the value obtained by means of the classical-trajectory calculation than is the MMA value of $(nD)^*$. Mason and Monchick[63] also demonstrated that inelastic energy exchange, due to the presence of rotational degrees of freedom, enters viscosity as a second-order effect and $(nD)^*$ as a first-order effect. Thus, it is safe to assume that the inelastic collisions have a marginally larger effect on the diffusion of the molecules rather than on the exchange of momentum and hence, resulting in A^* values that are a few percent larger for chain molecules than for spherical molecules.

As has been previously argued, at reduced temperatures higher than approximately $T^* = 5$ the transport coefficients are essentially determined by the effective repulsive potential. If the effective repulsive potentials for both viscosity and diffusion are the same, the ratio A^* would be constant. However, as illustrated in Figure 2, the index α of the effective repulsive potential is not the same for the two transport properties. For a sphere the effective potential for viscosity has a larger α, while for longer chains the converse is true and the effective potential for the diffusion coefficient has a larger α. Hence, for spheres interacting through a Lennard-Jones 12-6 potential the ratio A^* increases weakly with temperature for $T^* > 5$, while for chains consisting of more than 3 segments the ratio A^* decreases weakly with temperature.

It is interesting to note that for all the polyatomic molecules studied so far[14,17,45] A^* exhibits a similar temperature behavior as depicted in Figure 6(a). Figure 6(b) compares the behavior of A^* for CH_4 and CO_2 with the results obtained in this work for chain-like molecules. CH_4 and CO_2 were chosen out of the molecules studied as examples of molecules with the smallest and largest intermolecular potential anisotropy.

The calculations for real molecules were based on the *ab initio* potentials, so it is not straightforward to assign an appropriate value of the well-depth in order to adequately scale the temperature. As there is no single energy scaling parameter that corresponds to the well-depth of the Lennard-Jones 12-6 site-site potential, we have used the value corresponding to the well-depth of the spherically averaged *ab initio* potential. Hence, there remains a level of uncertainty in the T^* position of the A^* values of CH_4 and CO_2 depicted in Figure 6(b). However, it is the magnitude of A^* at high temperatures that we are primarily interested in. As we have already discussed, the magnitude of the higher-order viscosity correction factor is larger than that observed for real polyatomic gases. This is a direct result of the anisotropy of the potential dominating the angular momentum coupling contribution. For A^* all the indications are that the anisotropy only enters through inelastic collisions, which contribute to the effective cross sections, but do not have a dominant effect. Hence, at high reduced temperatures the values of A^* of CH_4 and CO_2 are approximately what we would expect based on geometric considerations. The temperature dependence of A^* for CH_4 and CO_2 resembles that for 1-segment and 2-segment chains, respectively.

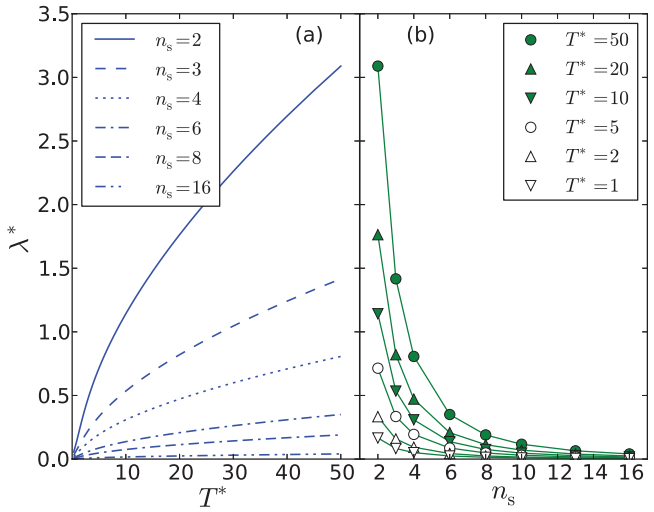

FIG. 7. Reduced thermal conductivity of rigid Lennard-Jones chains as a function of the reduced temperature T^* and the number of segments per chain n_s obtained using the second-order approximation.

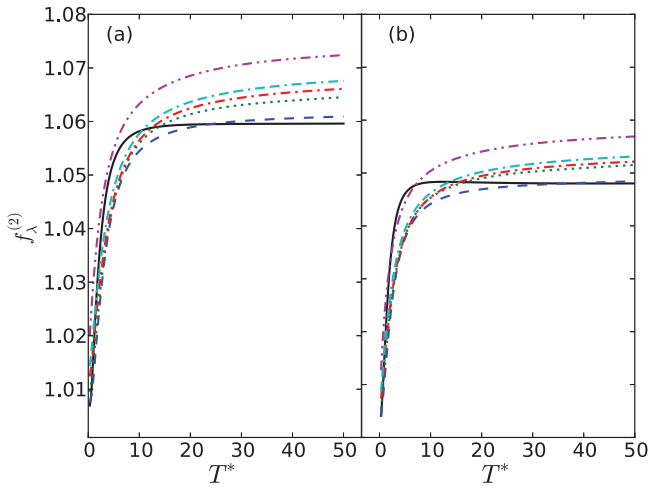

FIG. 8. (a) Second-order thermal conductivity correction factor $f_\lambda^{(2)}$ of rigid Lennard-Jones chains as a function of the reduced temperature T^*. (b) Contribution of the angular momentum coupling to the second-order thermal conductivity correction factor: $n_s = 2$ (-), $n_s = 3$ (--), $n_s = 4$ (· ·), $n_s = 6$ (- · -), $n_s = 8$ (-- ·), $n_s = 16$ (- · ·).

D. Thermal conductivity

The reduced thermal conductivity was calculated by means of the two-flux approach, Eq. (3). Figure 7(a) illustrates its behavior as a function of the reduced temperature T^* for a number of selected chains of different length, while Figure 7(b) illustrates the behavior as a function of the number of segments for a number of selected reduced temperatures. We observe a very similar behavior to that of the viscosity and diffusion coefficients. The increase in the chain length leads to a decrease in the thermal conductivity, while the increase in temperature leads to an increase. At any particular reduced temperature, the decrease in thermal conductivity does not obey any simple power law as a function of number of segments. At high reduced temperatures, the thermal conductivity is determined by the effective repulsive potential similar to what is observed for viscosity and self-diffusion.

The values of reduced thermal conductivity have also been calculated by means of the Thijsse approach, Eqs. (4) and (5). The agreement with the calculations based on the first-order two-flux approach (Eq. (3) with $f_\lambda^{(n)} = 1$) is excellent. The deviations increase slightly with increasing temperature, but never exceed 0.6% for any of the chain molecules studied. The variation of the deviations with chain length is negligible and is just outside the claimed uncertainty of the calculation. The current results are in agreement with the previous findings based on studies of small molecules (N_2, CO, CO_2, CH_4, H_2S, and C_2H_6),[15,18,20,44,46] where the two approaches for calculating thermal conductivity were equally effective. It is reassuring that the total-flux approach gives very good estimates of the first-order thermal conductivity even for highly eccentric molecules. This provides further evidence that a single cross section, $\mathfrak{S}(10E)$, is sufficient to describe closely the behavior of the thermal conductivity and can be used for correlating thermal conductivity of real fluids.

We next consider the contribution of the higher-order correction factor $f_\lambda^{(n)}$ to the thermal conductivity. Figure 8(a) illustrates the temperature dependence of the second-order thermal conductivity correction factors $f_\lambda^{(2)}$ for a number of selected chains of different length. The temperature dependence is similar to that observed for the viscosity correction factor, with a rapid increase followed by a levelling off at higher temperatures. However, the magnitude is much larger. The thermal conductivity correction factor reaches values of $1.06 - 1.07$ at the highest temperatures compared to $1.02 - 1.03$ for the viscosity correction. What is interesting is that the magnitude of the correction does not change monotonically with chain length, and the shortest chain studied, $n_s = 2$, displays a more rapid levelling off than that observed for longer chains. In order to rationalize the large magnitude observed we examine separately the influence of increasing the chain length on the second-order correction factor due to velocity polarization and that due to angular momentum coupling. The correction due to a velocity polarization shows the expected behavior, increasing both with temperature and chain length with a magnitude slightly larger than that observed for viscosity. However, the correction due to angular momentum coupling exhibits an unusual behavior for the 2-segment chain as illustrated in Figure 8(b). More puzzling is the magnitude of the correction of the order of 5% at high temperatures which has not been observed for any real gas studied to date. Nevertheless, a similarly high angular momentum correction factor ($f_\lambda^{(2)} = 1.051$) has been reported[11] for a model system consisting of spherocylinders of unit eccentricity, which corresponds to a 2-segment chain. The thermal conductivity in the second-order approximation, taking into account only the angular momentum coupling contribution, is given by Eq. (3) with each of the three cross sections $\mathfrak{S}(1010)$, $\mathfrak{S}\binom{1001}{1010}$, and $\mathfrak{S}(1001)$ replaced by the equivalent "second-order" cross

sections given by[15]

$$\left[\mathfrak{S}\begin{pmatrix}10st\\10s't'\end{pmatrix}\right]_2^{1200} = \mathfrak{S}\begin{pmatrix}10st\\10s't'\end{pmatrix} \times \left[1 - \frac{\bar{\mathfrak{S}}\begin{pmatrix}1200\\10st\end{pmatrix}\bar{\mathfrak{S}}\begin{pmatrix}1200\\10s't'\end{pmatrix}}{\mathfrak{S}\begin{pmatrix}10st\\10s't'\end{pmatrix}\bar{\mathfrak{S}}(1200)^{(1)}}\right]. \quad (9)$$

In this paper, we follow the standard notation[1,14,17] and the overbar is indicated only when the barred and unbarred cross sections differ. The angular momentum coupling correction is dominated by the production cross section $\bar{\mathfrak{S}}\binom{1200}{1001}$, which is much larger than the production cross section $\bar{\mathfrak{S}}\binom{1200}{1010}$. This is not surprising since the former is more influenced by inelastic collisions. This observation led Viehland and co-workers[43] to neglect the latter when deriving their approximate expressions for the influence of the angular momentum coupling on thermal conductivity. Consequently, the second-order angular momentum polarization correction primarily influences the cross sections $\mathfrak{S}(1001)$ and $\mathfrak{S}\binom{1001}{1010}$, effectively decreasing the former and increasing the latter. The overall effect is to increase the thermal conductivity, as can be most easily seen from Eqs. (4) and (5). Thus, the large magnitude observed in Figure 8 is directly related to the large effect that the second-order correction has on the $\mathfrak{S}(1001)$ and $\mathfrak{S}\binom{1001}{1010}$ cross sections. A similar behavior was observed for real molecules when they were approximated as rigid rotors.[15,45,47] However, when the rigid-rotor approximation was relaxed and the molecules were allowed to transport energy in the vibrational modes, the effect of the second-order correction on the two cross sections decreased. This led to a smaller overall contribution of the second-order thermal conductivity correction for real gases than has been observed here.[15,45,47] It is not clear if these observations can be generalized or if they are due to a fortuitous cancellation of individual contributions. If the previous results based on studies of the thermal conductivity of CO_2 and CH_4 can be generalized, then one can postulate that the second-order thermal conductivity correction factors are unusually large because the chain molecules are treated as rigid rotors. If the chain molecules are made flexible and allowed to vibrate, the second-order correction would be smaller. It remains to be seen if real gases made of long chain molecules display large second-order correction factors for the angular momentum coupling, or if it is simply an artifact of treating chains as rigid rotors.

The ratios of transport properties play an important part in our understanding of the interconnections between different properties at the level of kinetic theory and can also provide a useful way of predicting one property from the knowledge of another. In Sec. III C, we examined the parameter A^*, while here we focus on the Prandtl number,

$$Pr = \frac{C_p\eta}{m\lambda} = \frac{7}{2}\frac{\eta^*}{n_s\lambda^*}, \quad (10)$$

where C_p is the isobaric heat capacity and the second equation is valid only for the linear rigid chains considered in this work.

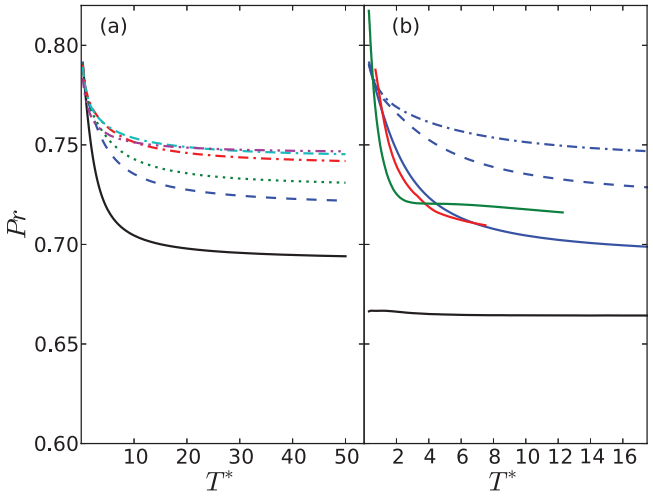

FIG. 9. (a) Prandtl number of rigid Lennard-Jones chains as a function of the reduced temperature T^*: $n_s = 2$ (-), $n_s = 3$ (--), $n_s = 4$ (· ·), $n_s = 6$ (- · -), $n_s = 8$ (-- ·), $n_s = 16$ (- · ·). (b) Comparison of the Prandtl number for Lennard-Jones spheres (black solid line), CO_2 (red solid line), and CH_4 (green solid line) with that for Lennard-Jones chains (blue lines): $n_s = 2$ (-), $n_s = 3$ (--), $n_s = 6$ (- · -).

For monatomic species at temperatures where electronic excitations are negligible, the Prandtl number is exactly 2/3 in the first-order approximation. Its temperature dependence arises from the ratio of the higher-order correction factors. Figure 9(a) illustrates the temperature dependence of the Prandtl number for a number of selected chains of different length. As is observed for real fluids, the Prandtl number of chains also decreases with increasing temperature approaching a constant value at higher temperatures. The temperature dependence is strongest for the 2-segment chain and it decreases steadily as the length of the chain increases. At low reduced temperatures the Prandtl number converges to a value of 0.8 irrespective of the chain length, while at higher temperatures the longer chains converge to a Prandtl number of approximately 0.75. The Prandtl numbers of CO_2 and CH_4, shown in Figure 9(b), exhibit a stronger temperature dependence at lower temperatures, but are of similar magnitudes as the Prandtl numbers of the chains.

IV. SUMMARY AND CONCLUSIONS

The shear viscosity, the self-diffusion coefficient, and the thermal conductivity have been calculated for a dilute gas in the reduced temperature range $0.3 - 50$. The molecules of the gas were modelled as rigid chains consisting of a number of spherical segments, that interact through a combination of site-site Lennard-Jones 12-6 potentials. The calculations were performed for chains consisting of 1, 2 ,3 ,4, 5, 6, 7, 8, 10, 13, and 16 segments.

All three transport properties show a similar behavior, increasing with temperature and decreasing with chain length. At high temperatures, the observed temperature dependence corresponds to that of molecules interacting through a spherical, repulsive potential. Hence, it can be argued that at high temperatures an effective repulsive potential governs the transport properties of a gas. The hardness of the effective

potential increases with the chain length, supporting the recent thermodynamic studies based on the SAFT-Mie EOS, that also indicate that the larger molecules interact through a potential with an increasingly more repulsive wall than the smaller molecules.

No simple scaling of transport properties was observed with the number of segments. Hence, the conclusion based on studies of spherocylinders that the decrease in transport properties with increasing chain length can be solely attributed to the increase in projected area and mass is not supported.

The higher-order correction factors have been calculated up to the third order for viscosity and up to the second order for thermal conductivity. The observed temperature dependence is similar to that observed for real systems, with the correction factors displaying a rapid increase at low reduced temperatures and levelling off at higher reduced temperatures. The dependence of the correction factors on the number of segments shows the expected behavior for viscosity, with the correction factor broadly increasing with the length of the chain. For thermal conductivity, some unusual behavior has been observed typified by the 2-segment chain. The contribution to the correction factor due to the velocity coupling is small, of the order of $1\% - 2\%$ at most, implying that the convergence in the velocity basis function expansion is fast. However, the magnitude of the contribution to the correction factor due to angular momentum coupling is much larger, reaching values of 5.7% for thermal conductivity. Although such high values have been observed for other model systems, where the rotation is the main way in which these molecules relax,[11] for the real gases studied so far the values are much smaller. Based on the calculations for real gases a hypothesis was put forward that for non-rigid chains, that can vibrate, the correction will be smaller.

Two quantities that measure the ratio of transport properties, namely, A^* and the Prandtl number, have also been examined. They display a weak temperature dependence above approximately $T^* = 1 - 2$ and are weak functionals of the length of the chain. The latter indicates a weak dependence on the anisotropy of the potential. Analogous behavior was observed for monatomic systems were A^* is only weakly dependent on the intermolecular potential.

The comparison of the present calculations with those carried out by molecular dynamics simulations indicates a good agreement for shorter chains, within the claimed accuracy, while for longer chains differences slightly larger than the claimed accuracy are observed.

It is interesting to compare the results for chains with the behavior of real systems, where so far similar calculations have been based on smaller molecules. The comparison shows that for the transport properties studied in this work, which are only weakly dependent on the anisotropy of the potential, the proposed chain model with intermolecular sites at the center of each segment, can be used to adequately model the real molecules studied so far. Thus, one could model, on geometric grounds, the CO_2 molecule as a 2-segment chain and the CH_4 molecule as a 1-segment chain. However, if we are interested in a property that is primarily determined by the angular momentum coupling and is thus strongly dependent on anisotropy (e.g., the higher-order correction factor for the angular momentum coupling) the present chain model is too anisotropic. To model CO_2 as a 2-segment chain, one would have to reduce the site-site separation.

ACKNOWLEDGMENTS

N.R. would like to acknowledge that his work was supported by the Qatar Carbonates and Carbon Storage Research Centre (QCCSRC). QCCSRC is funded jointly by Qatar Petroleum, Shell, and the Qatar Science and Technology Park.

[1] F. R. W. McCourt, J. J. M. Beenakker, W. E. Köhler, and I. Kuščer, *Nonequilibrium Phenomena in Polyatomic Gases* (Oxford Science, 1990), Vol. 1.
[2] S. Chapman and T. G. Cowling, *The Mathematical Theory of Non-Uniform Gases: An Account of the Kinetic Theory of Viscosity, Thermal Conduction and Diffusion in Gases* (Cambridge University Press, 1991).
[3] F. B. Pidduck, Proc. R. Soc. London, Ser. A **101**, 101 (1922).
[4] J. H. Jeans, Philos. Trans. R. Soc. London, Ser. A **196**, 397 (1901).
[5] J. S. Dahler, J. Chem. Phys. **30**, 1447 (1959).
[6] J. S. Dahler and N. F. Sather, J. Chem. Phys. **38**, 2363 (1963).
[7] S. I. Sandler and J. S. Dahler, J. Chem. Phys. **43**, 1750 (1965).
[8] C. F. Curtiss and C. Muckenfuss, J. Chem. Phys. **26**, 1619 (1957).
[9] C. Muckenfuss and C. F. Curtiss, J. Chem. Phys. **29**, 1257 (1958).
[10] P. M. Livingston and C. F. Curtiss, J. Chem. Phys. **31**, 1643 (1959).
[11] S. I. Sandler and J. S. Dahler, J. Chem. Phys. **44**, 1229 (1966).
[12] R. Hellmann, "*Ab initio* potential energy surface for the nitrogen molecule pair and thermophysical properties of nitrogen gas," Mol. Phys. (in press).
[13] E. L. Heck and A. S. Dickinson, Physica A **217**, 107 (1995).
[14] S. Bock, E. Bich, E. Vogel, A. S. Dickinson, and V. Vesovic, J. Chem. Phys. **117**, 2151 (2002).
[15] S. Bock, E. Bich, E. Vogel, A. S. Dickinson, and V. Vesovic, J. Chem. Phys. **120**, 7987 (2004).
[16] S. Bock, E. Bich, E. Vogel, A. S. Dickinson, and V. Vesovic, J. Chem. Phys. **121**, 4117 (2004).
[17] R. Hellmann, E. Bich, E. Vogel, A. S. Dickinson, and V. Vesovic, J. Chem. Phys. **129**, 064302 (2008).
[18] R. Hellmann, E. Bich, E. Vogel, A. S. Dickinson, and V. Vesovic, J. Chem. Phys. **130**, 124309 (2009).
[19] R. Hellmann, E. Bich, E. Vogel, A. S. Dickinson, and V. Vesovic, J. Chem. Phys. **131**, 014303 (2009).
[20] R. Hellmann, E. Bich, E. Vogel, and V. Vesovic, Phys. Chem. Chem. Phys. **13**, 13749 (2011).
[21] G. Galliéro, Fluid Phase Equilib. **224**, 13 (2004).
[22] G. Galliéro, C. Boned, and A. Baylaucq, Ind. Eng. Chem. Res. **44**, 6963 (2005).
[23] G. Galliéro, M. Bugel, B. Duguay, and F. Montel, J. Non-Equilib. Thermodyn. **32**, 251 (2007).
[24] M. Bugel and G. Galliéro, Chem. Phys. **352**, 249 (2008).
[25] G. Galliéro, C. Boned, A. Baylaucq, and F. Montel, Phys. Rev. E **73**, 061201 (2006).
[26] G. Galliéro, C. Boned, A. Baylaucq, and F. Montel, Chem. Phys. **333**, 219 (2007).
[27] G. Galliéro, T. Lafitte, D. Bessiéres, and C. Boned, J. Chem. Phys. **127**, 184506 (2007).
[28] G. Galliéro and C. Boned, J. Chem. Phys. **129**, 074506 (2008).
[29] G. Galliéro, M. M. Piñeiro, B. Mendiboure, C. Miqueu, T. Lafitte, and D. Bessiéres, J. Chem. Phys. **130**, 104704 (2009).
[30] G. Galliéro, C. Nieto-Draghi, C. Boned, J. B. Avalos, A. D. Mackie, A. Baylaucq, and F. Montel, Ind. Eng. Chem. Res. **46**, 5238 (2007).
[31] G. Galliéro and C. Boned, Fluid Phase Equilib. **269**, 19 (2008).
[32] G. Galliéro and C. Boned, Phys. Rev. E **79**, 021201 (2009).
[33] G. Galliéro and C. Boned, Phys. Rev. E **80**, 061202 (2009).
[34] G. Galliéro, J. Chem. Phys. **133**, 074705 (2010).
[35] S. Delage Santacreu, G. Galliéro, M. Odunlami, and C. Boned, J. Chem. Phys. **137**, 204306 (2012).
[36] T. K. Patra, A. Hens, and J. K. Singh, J. Chem. Phys. **137**, 084701 (2012).
[37] Y.-X. Yu and G.-H. Gao, Fluid Phase Equilib. **166**, 111 (1999).

[38]Y.-X. Yu and G.-H. Gao, Int. J. Thermophys. **21**, 57 (2000).
[39]Y.-X. Yu and G.-H. Gao, Fluid Phase Equilib. **179**, 165 (2001).
[40]X.-G. Zhang and Y.-X. Yu, Fluid Phase Equilib. **295**, 237 (2010).
[41]J. H. Ferziger and H. G. Kaper, *Mathematical Theory of Transport Processes in Gases* (North-Holland, Amsterdam, 1972).
[42]Y. Kagan and L. Maksimov, Sov. Phys. JETP **14**, 604 (1962).
[43]L. A. Viehland, E. A. Mason, and S. I. Sandler, J. Chem. Phys. **68**, 5277 (1978).
[44]G. C. Maitland, M. Mustafa, and W. A. Wakeham, J. Chem. Soc., Faraday Trans. 2 **79**, 1425 (1983).
[45]R. Hellmann, E. Bich, E. Vogel, and V. Vesovic, J. Chem. Eng. Data **57**, 1312 (2012).
[46]B. J. Thijsse, G. W. 'T Hooft, D. A. Coombe, H. F. P. Knaap, and J. J. M. Beenakker, Physica A **98**, 307 (1979).
[47]J. Millat, V. Vesovic, and W. A. Wakeham, Physica A **148**, 153 (1988).
[48]S. Hendl, J. Millat, V. Vesovic, E. Vogel, and W. A. Wakeham, Int. J. Thermophys. **12**, 999 (1991).
[49]E. L. Heck and A. S. Dickinson, Comput. Phys. Commun. **95**, 190 (1996).
[50]See supplementary material at http://dx.doi.org/10.1063/1.4793221 for electronic files that contain these tables.
[51]G. C. Maitland, V. Vesovic, and W. A. Wakeham, Mol. Phys. **54**, 287 (1985).
[52]G. C. Maitland, V. Vesovic, and W. A. Wakeham, Mol. Phys. **54**, 301 (1985).
[53]C. Avendaño, T. Lafitte, A. Galindo, C. S. Adjiman, G. Jackson, and E. A. Müller, J. Phys. Chem. B **115**, 11154 (2011).
[54]T. Lafitte, C. Avendaño, V. Papaioannou, A. Galindo, C. S. Adjiman, G. Jackson, and E. A. Müller, Mol. Phys. **110**, 1189 (2012).
[55]C. Avendaño, T. Lafitte, A. Galindo, C. S. Adjiman, E. A. Müller, and G. Jackson, "SAFT-γ Force Field for the Simulation of Molecular Fluids: 2. Coarse-Grained Models of Greenhouse Gases, Refrigerants, and Long Alkanes," J. Phys. Chem. B (unpublished).
[56]A. Haslam, personal communication (1 October 2012).
[57]G. Galliéro, C. Boned, and J. Fernández, J. Chem. Phys. **134**, 064505 (2011).
[58]G. Galliéro, personal communication (16 November 2012).
[59]G. C. Maitland, M. Rigby, E. B. Smith, and W. A. Wakeham, *Intermolecular Forces: Their Origin and Determination* (Clarendon, Oxford, 1981).
[60]V. Vesovic, S. Bock, E. Bich, E. Vogel, and A. S. Dickinson, Chem. Phys. Lett. **377**, 106 (2003).
[61]E. L. Heck, A. S. Dickinson, and V. Vesovic, Chem. Phys. Lett. **240**, 151 (1995).
[62]E. L. Heck, A. S. Dickinson, and V. Vesovic, Chem. Phys. Lett. **204**, 389 (1993).
[63]E. A. Mason and L. Monchick, J. Chem. Phys. **36**, 1622 (1962).